



HAL
open science

Generation of XUV spectral continua from relativistic plasma mirrors driven in the near-single-cycle limit

Frederik Böhle, Maxence Thévenet, Maïmouna Bocoum, Aline Vernier, Stefan Haessler, Rodrigo Lopez-Martens

► **To cite this version:**

Frederik Böhle, Maxence Thévenet, Maïmouna Bocoum, Aline Vernier, Stefan Haessler, et al.. Generation of XUV spectral continua from relativistic plasma mirrors driven in the near-single-cycle limit. Journal of Physics: Photonics, 2020, 2, pp.034010. 10.1088/2515-7647/ab9715 . hal-02978239

HAL Id: hal-02978239

<https://hal.science/hal-02978239>

Submitted on 26 Oct 2020

HAL is a multi-disciplinary open access archive for the deposit and dissemination of scientific research documents, whether they are published or not. The documents may come from teaching and research institutions in France or abroad, or from public or private research centers.

L'archive ouverte pluridisciplinaire **HAL**, est destinée au dépôt et à la diffusion de documents scientifiques de niveau recherche, publiés ou non, émanant des établissements d'enseignement et de recherche français ou étrangers, des laboratoires publics ou privés.

PAPER • OPEN ACCESS

Generation of XUV spectral continua from relativistic plasma mirrors driven in the near-single-cycle limit

To cite this article: Frederik Böhle *et al* 2020 *J. Phys. Photonics* **2** 034010

View the [article online](#) for updates and enhancements.



PAPER

OPEN ACCESS


RECEIVED
10 March 2020REVISED
6 May 2020ACCEPTED FOR PUBLICATION
27 May 2020PUBLISHED
6 July 2020

Original Content from
this work may be used
under the terms of the
[Creative Commons
Attribution 4.0 licence](#).

Any further distribution
of this work must
maintain attribution to
the author(s) and the title
of the work, journal
citation and DOI.



Generation of XUV spectral continua from relativistic plasma mirrors driven in the near-single-cycle limit

Frederik Böhle¹, Maxence Thévenet², Maïmouna Bocoum¹, Aline Vernier¹, Stefan Haessler¹ 
and Rodrigo Lopez-Martens¹

¹ Laboratoire d'Optique Appliquée, CNRS, Ecole Polytechnique, ENSTA Paris, Institut Polytechnique de Paris, 181 chemin de la
Hunière et des Joncherettes 91120 Palaiseau, France

² Lawrence Berkeley National Laboratory, Berkeley, California 94720, United States of America

E-mail: stefan.haessler@ensta-paris.fr

Keywords: attosecond pulses, plasmas, surface high-harmonic generation

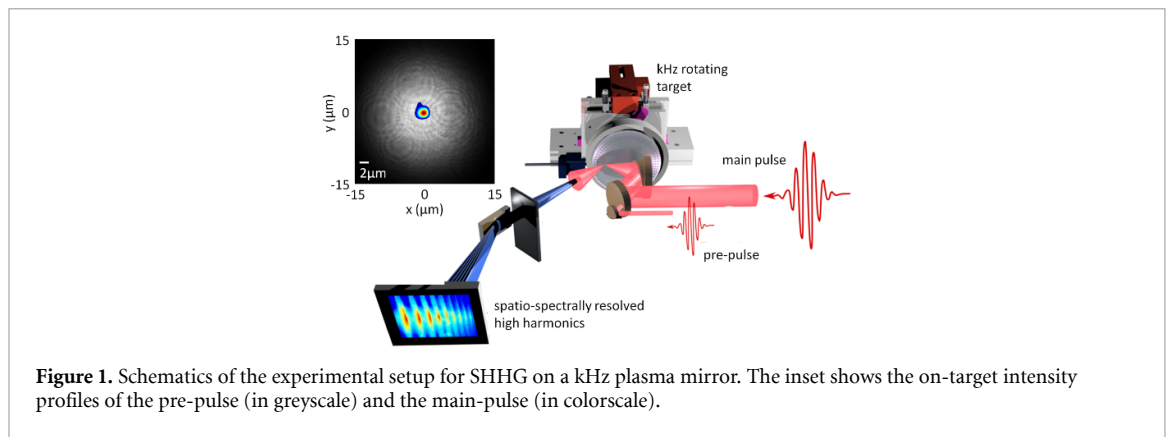
Abstract

We present experiments using relativistic-intensity 1.5-cycle laser fields at 1 kHz repetition rate to drive surface high-harmonic generation (SHHG) from surface plasmas with controlled density gradient. As a function of the driving pulse carrier-envelope phase (CEP), we observe a transition from a modulated to a continuous SHHG spectrum, indicating the transition from double to isolated attosecond pulse emission. Single shot-acquisitions of XUV spectral continua support the emission of isolated attosecond pulses with an isolation degree of between 10 and 50 for the majority of the driving pulse CEPs. 2D Particle-in-cell simulations corroborate this interpretation and predict percent-level efficiencies for the generation of an isolated attosecond pulse even without spectral filtering.

1. Introduction

Surface high-harmonic generation (SHHG) from relativistic plasma mirrors has long been recognized as an efficient route to high-energy intense attosecond XUV pulses [1–3]. The phenomenon occurs when focusing an high-contrast visible to infrared driving laser in oblique incidence onto an optically polished solid target [4]. Already the rising edge of a highly intense laser pulse creates a solid-density plasma on the target surface. If a sufficiently steep (scale length L of a small fraction of the driving wavelength) plasma density gradient is retained, the incident light is nonlinearly reflected into a high-quality beam [5, 6] with its spectrum extended into the XUV corresponding in the time domain to the emission of attosecond pulses. Plasma mirrors complement the established attosecond pulse generation method via high-harmonic generation (HHG) in gases at much lower intensities in the strong-field regime, since they exhibit no inherent limitation for the driving intensity. They thus allow full exploitation of ultra-high intensity lasers in order to convert an extremely large number of photons from a femtosecond laser into attosecond XUV pulses. In strongly relativistic conditions, $a_0 \gg 1$, this is expected to occur with extremely high, percent-level conversion efficiencies [1, 7]. The laser-to-XUV conversion efficiencies of $\sim 10^{-4}$ currently experimentally observed for plasma mirrors with $a_0 \sim 1$ [3, 8–10] already rival the highest demonstrated efficiencies of gas HHG [11, 12]. This makes SHHG on plasma mirrors one of the paramount candidates for greatly enhancing the available energy of attosecond XUV pulses.

The interaction conditions on plasma mirrors may be roughly divided into a sub-relativistic and a relativistic regime, corresponding to a normalised vector potential $a_0 = \sqrt{I[\text{Wcm}^{-2}] \lambda_0^2 [\mu\text{m}^2]} / (1.37 \times 10^{18}) < 1$ and > 1 , respectively, where I is the laser intensity and λ_0 the central wavelength. These regimes are associated with two distinct SHHG mechanisms. In sub-relativistic conditions, coherent wake emission (CWE) [4] dominates. This process requires an extremely steep plasma-vacuum interface ($L \sim \lambda/100$) and typically generates a spectral plateau extending up to the maximum plasma frequency given by the density of the solid target, which corresponds to ≈ 30 eV photon energy for an SiO_2 target.



For relativistic driving intensities, the dominating mechanism is described by a three-step push–pull–emission process [13, 14] repeating once per driving laser period. (i) ‘Push’: The incident laser field first pushes electrons through the magnetic force into the plasma, piling up a dense electron bunch and creating a corresponding restoring internal plasma field. (ii) ‘Pull’: As the laser field changes sign, the combined plasma and laser fields accelerate the electron bunch to a relativistic velocity towards the vacuum. (iii) ‘Emission’: High-harmonic emission is then described either as a pure phase modulation of the incident laser field through a temporal compression upon reflection on the relativistically moving critical-density plasma surface (‘relativistic oscillating mirror’) [1, 15, 16], or as a coherent synchrotron emission (CSE) from the relativistically moving dense electron bunch as it gets accelerated orthogonally by the laser electric field [7, 17]. The generated spectra have a typical power-law decay $\propto \omega^{-p}$, with $p \approx 1.3\text{--}3$ depending on the conditions, and for sufficiently high driving intensity can extend well beyond the spectral cutoff of the CWE mechanism. The optimal plasma density gradient scale length for this process is found to be $L \approx \lambda/10$ [6, 8, 18].

Temporally gating this process to a single dominant driving laser period and thus limiting SHHG to the emission of a single attosecond pulse remains extremely challenging with ultra-high-intensity laser systems, i.e. of terawatt to petawatt class with extreme temporal contrast of $\geq 10^{10}$, since the known methods from gas HHG [19] are not easily transferred. Proof-of-principle demonstrations of polarization-gating [20–23] and the attosecond lighthouse method [24, 25] have been reported, but have the drawback of being rather costly in terms of achievable driving intensity.

More efficient but technically very challenging is intensity-gating through reduction of the laser pulse duration. For this approach, 2-cycle pulses with ~ 10 mJ energy have been generated by optical parametric chirped pulse amplifier (OPCPA) chains with 10 Hz repetition rate [26, 27]. These have been applied to generate SHHG with spectrally overlapping harmonics [3, 28] – the essential prerequisite for an isolated attosecond pulse. Simulations supporting these experiments [3] or a spectral interferometry analysis of SHHG spectra presenting a beating pattern of three unevenly spaced attosecond pulses [28] have led to the conclusion that for the optimal carrier-envelope phase (CEP) value, an isolated attosecond pulse with an isolation degree ≈ 25 (defined as main-to-satellite pulse temporal intensity ratio) can be generated after spectral selection of harmonics > 40 eV. The vast majority of driving pulse CEPs did however lead to the emission of a double or triple attosecond pulse train.

Our approach to intensity gating is based on the spatio-temporal confinement of few-mJ-energy pulses to a focal volume comparable to the laser wavelength cubed [29], which enables relativistic interaction conditions at kHz-repetition rate [30, 31]. To this end, we have developed a 1-kHz repetition rate laser that routinely delivers 3.5-fs (1.5-cycles of the 720-nm central wavelength) pulses with 1 TW peak power, based on a high-contrast Ti:sapphire double-CPA system followed by a power-scaled stretched-hollow-core-fiber compressor [32–34]. Here we report on SHHG from relativistic plasma mirrors driven by this 1.5-cycle laser, leading to XUV continua (10–25 eV) with a degree of residual spectral modulation varying as a function of the laser CEP and supporting an isolated attosecond pulse with an isolation degree $\gtrsim 25$ for half of the 2π -CEP-range. We also theoretically predict that such a driver pulse should allow the generation of an attosecond pulse with an isolation degree of 10 without any spectral filtering.

2. Experiments

For SHHG, a vacuum beamline sends the 3.5-fs laser pulses onto a rotating optically flat solid target with a controlled plasma density gradient. As illustrated in figure 1, the p-polarized laser is focused down to a $1.8\text{-}\mu$

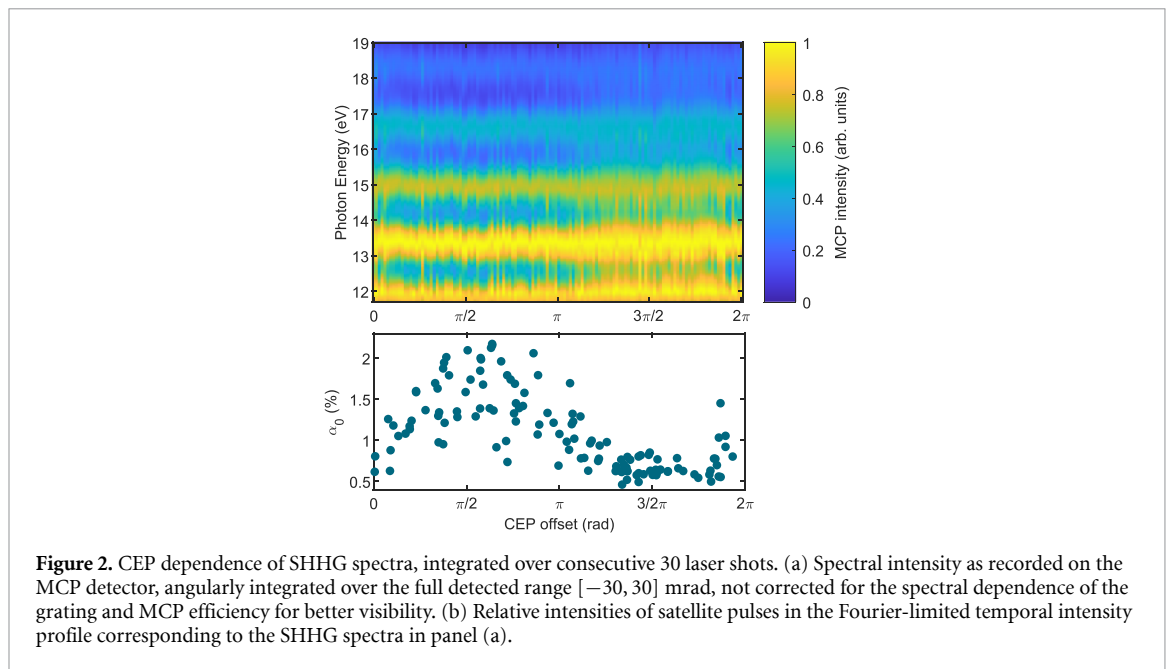


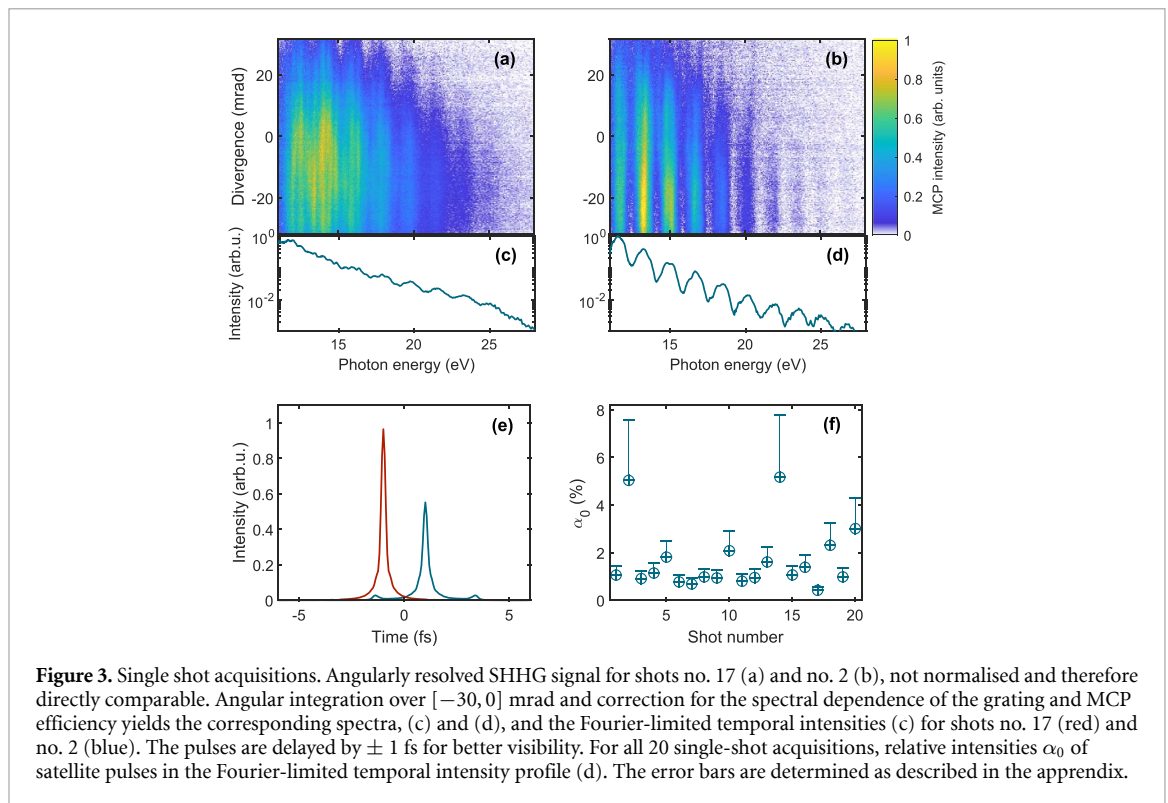
Figure 2. CEP dependence of SHHG spectra, integrated over consecutive 30 laser shots. (a) Spectral intensity as recorded on the MCP detector, angularly integrated over the full detected range $[-30, 30]$ mrad, not corrected for the spectral dependence of the grating and MCP efficiency for better visibility. (b) Relative intensities of satellite pulses in the Fourier-limited temporal intensity profile corresponding to the SHHG spectra in panel (a).

m FWHM spot using an $f/1.5$, 30° off-axis parabola onto the fused silica target at an incidence angle of $\theta = 55^\circ$. With a pulse energy of 2.6 mJ on target, this yields, in absence of spatio-temporal distortions, a peak intensity of 1.0×10^{19} W/cm², corresponding to a peak normalised vector potential of $a_0 = 2.0$. Note however, that the true on-target intensity is most likely lower due to uncharacterized spatio-temporal couplings. A spatially superposed pre-pulse, created by picking off and then recombining $\approx 4\%$ of the main pulse through holey mirrors, is focused to a much larger $13 \mu\text{m}$ FWHM spot in order to generate a homogeneous plasma expanding into vacuum. The plasma density scale length L was controlled by setting a delay of 2 ps between this pre-pulse and the main driving pulse and measured to be $L = \lambda/20$ using spatial-domain interferometry [35]. This optimizes the conditions for ROM SHHG emission [6, 31] and we will in the following consider the experimentally observed SHHG emission as such although its photon energy range is below the CWE spectral cutoff.

The emitted harmonic radiation in the specular direction is then recorded, as a function of the driving near-single-cycle laser waveform, using a home-made XUV spectrometer, including a gold-coated flat-field grating (Hitachi 001-0639, 600 lines/mm, 85.3° incidence), which lets the beam freely expand in the vertical dimension and images in the horizontal dimension the source point on the plasma-mirror surface onto a coupled micro-channel-plate (MCP) and phosphor screen detector (Photonis APD, $79 \times 97 \text{ mm}^2$, with single NiChrome-coated MCP and P46 phosphor screen). The MCP is time-gated for ≈ 250 ns synchronously with the laser pulses so as to suppress longer background plasma emission. The phosphor screen is finally imaged by a charged-coupled-device (CCD) camera to record angularly resolved ($[-30, 30]$ mrad) SHHG spectra. The spectral dependence of the grating and MCP efficiencies as supplied by the manufacturers can be corrected for in order to convert the signal recorded on the MCP into the SHHG spectral intensity.

The CEP of the driving pulses was measured with a home-built $f-2f$ spectral interferometer integrating over 15 laser shots. Since our 3.5-fs laser pulses already have an octave-spanning spectral bandwidth this did not include additional spectral broadening which could couple pulse energy fluctuations to phase measurement errors. The laser oscillator was CEP-locked, but the $f-2f$ measurement did not feed back to a slow CEP locking loop. The residual random CEP noise over a 200-ms time window was observed to be $\lesssim 500$ mrad on top of a slow quasi-linear CEP drift of ≈ 600 mrad/s.

This allows us to safely assume that the CEP was sufficiently stable during short bursts of 30 consecutive pulses, over which we integrated to record SHHG spectra. A series of such 30-ms long acquisitions were recorded in ≈ 4 s intervals, so that the CEP can be considered random from one recorded spectrum to the next. The simultaneously recorded relative CEP is then used to tag the SHHG spectra which yields the CEP-dependence shown in figure 2(a). Clearly, the harmonic spectral modulation depth is a smooth function of the CEP offset and almost completely disappears for about half of all driving pulse waveforms around a relative CEP offset of $\approx 3\pi/2$. Note that without CEP-tagging, the successively recorded SHHG spectra present random variations, which reassures us in the conclusion that the observed variations are due to the varying CEP of the 3.5-fs driving pulses. Fluctuations of other parameters such as pulse duration and energy are very small ($< 2\%$) and cannot account for the observed variability.



All our recorded spectra are continua in the sense that the spectrally large harmonics partially overlap. The varying spectral modulation depth suggests, in the time domain, a varying isolation degree of the dominant attosecond pulse relative to neighboring satellite pulses spaced by approximately one laser period of 2.4 fs. In order to quantify this variation, we consider the Fourier-limited temporal intensity profiles corresponding to the measured SHHG spectra (from 11 to 29 eV, corrected for the spectral dependence of the XUV grating efficiency and the MCP response). This necessarily yields symmetric temporal profiles which for our data correspond to a dominating central attosecond pulse surrounded on either side by two equal weaker satellite pulses (cf the profiles shown for single shot acquisitions in figure 3).

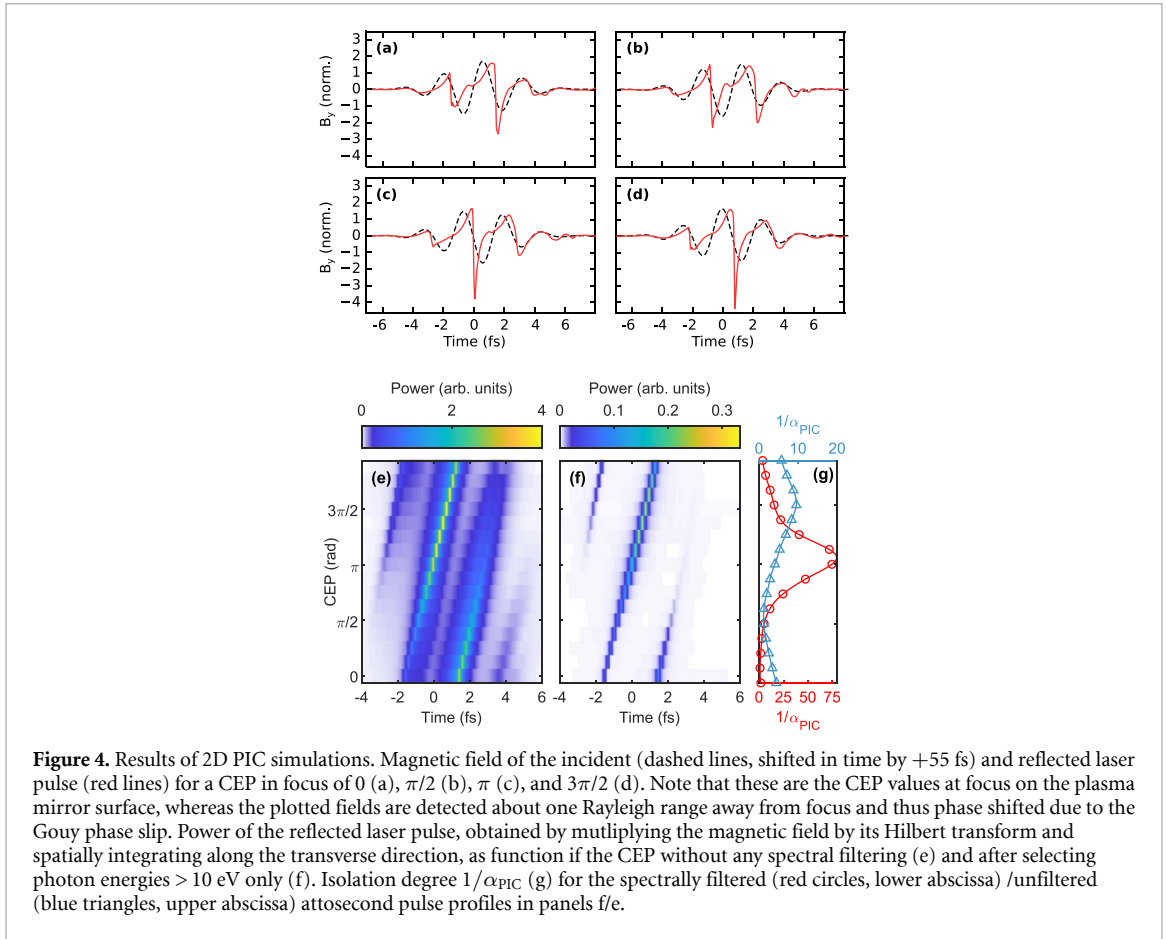
In figure 2(b), we plot the CEP-dependence of the peak intensity α_0 of the satellite pulse located at ≈ 2.45 fs normalised to that of the main central pulse in the train. The result confirms our conclusion from the qualitative discussion of the modulation depth visible in figure 2(a): the spectral modulation depth varies smoothly as a function of the driving pulse CEP and is minimal for about half of all CEP values.

The satellite pulse intensities α_0 are all so small (between 0.5 and 2%) that one may want to classify the temporal profiles as isolated attosecond pulses for all CEPs. Of course, this would be a precipitated claim and any statement about a temporal profile deduced only from a spectral intensity requires justified assumptions about the spectral phase. We will discuss this point in section 4. For now, we consider α_0 only as a quantitative measure for the continuous nature of the recorded SHHG spectra.

Since the data in figure 2 are obtained by integrating over 30 consecutive pulses at 1 kHz, any fast jitter of the interaction conditions, notably the CEP, could have washed out the harmonic spectral modulation leading to its underestimation [36].

We therefore made a series of 20 single-shot acquisitions in ≈ 4 s intervals, i.e. again for randomly varying CEP. Figures 3(a) and (b) shows the strikingly different angularly resolved SHHG spectra for two different shots. We can confirm that even in single-shot mode, we observe spectral continua with almost no harmonic spectral modulation. We also confirm our expectation that the absence of averaging in single-shot measurements allows us to observe much deeper harmonic spectral modulations for some shots.

Figures 3(c) and (d) analyze the harmonic spectra after angular integration over the range $[-30, 0]$ mrad, i.e. over the beam center only. This reduces possible contributions from more divergent CWE harmonics in the harmonic beam periphery (cf the discussion in section 4) as well as the possible influence of spatial beam distortions due to aberrations in the harmonic beam imaging system. In figures 3(a) and (b), it is clearly apparent that the continuous spectrum contains more energy than the modulated one. If the spectral continua indeed correspond to isolated attosecond pulses, then this difference is further amplified by concentrating that energy into a single pulse, which leads to the different peak intensities in the Fourier-limited temporal intensity profiles shown in figures 3(c) for the same selected shots as in figures 3(a)



and (b). Figure 3(d) shows the α_0 found from the Fourier-limited temporal intensity profiles for all 20 shots. Clearly, the vast majority of shots presents very low spectral modulations : e.g. for 9 out of the 20 pulses $\alpha_0 < 1\%$, and only for 3 pulses $\alpha_0 > 2.5\%$. On average over our single-shot acquisitions, we find an $\approx 30\%$ higher peak intensity of the Fourier-limited temporal profiles for the spectral continua with $\alpha_0 < 1\%$ compared to the modulated spectra with $\alpha_0 > 2.5\%$.

3. 2D Particle-in-cell simulations

In order to interpret our experimental results and support the discussion of the real temporal profiles, we performed a series of 2D particle-in-cell (PIC) simulations using the Warp code [37] with a Yee Maxwell solver. The parameters are chosen to approximately mimic the experimental conditions: The laser impinges at an angle of incidence of 55° onto a plasma with exponential density gradient of scale length $L = \lambda/10$ and a peak plasma density of $400n_c$, with the critical density n_c at 800 nm. The 3.5-fs FWHM Gaussian pulse with central wavelength of $\lambda = 800$ nm and varying CEP is focused to a $1.8\text{-}\mu\text{m}$ FWHM Gaussian spot to a peak intensity of 8.5×10^{18} W/cm², corresponding to $a_0 = 2$. In this regime, the paraxial approximation is not valid, and the pulse envelope varies rapidly compared to the laser period. To avoid errors associated with these approximations, the Gaussian laser pulse was constructed at focus in vacuum and back-propagated as part of the simulation initialization. That way, when the simulation starts and the laser pulse propagates towards the target, the E and B fields at focus (i.e. on the target surface) are those of a Gaussian laser pulse.

The simulations used 16 particles per cell. The simulation box had a size of $60\ \mu\text{m} \times 25\ \mu\text{m}$ with a grid step size of $\lambda/400$ and boundaries absorbing all fields (perfectly matched layer) and particles.

The dramatic effect of the CEP is evident in the comparison of the incident and reflected laser fields obtained in these simulations shown in figure 4(a)–(d). The fields are defined such that positive B-fields correspond to the ‘push’ phase of the relativistic SHHG process discussed in the introductory section; negative B-fields therefore correspond to the ‘pull’ phase. The CEP values considered in figure 4(a)–(d) thus represent different balances of the pushing and pulling laser field cycles: a CEP of 0 causes the strongest possible field during a ‘push’ phase, CEP = $\pi/2$ leads to two effective field cycles, with a stronger field in the ‘pull’ or ‘pull’ phase, respectively, CEP = π causes the strongest possible field during a ‘pull’ phase, and finally CEP = $3\pi/2$ leads to a single effective field cycle with equally strong fields during the ‘push’ and ‘pull’ phases.

Clearly, the latter two situations lead to the strongest temporal compression of a single dominant field cycle in the reflected pulse. The enhanced peak fields are compatible with the relativistic electron spring [13, 14] or coherent synchrotron emission [7, 17] models, where SHHG does not only result from a mere phase modulation but from reemission of energy stored in the compressed plasma.

Multiplying the calculated reflected B-fields by their Hilbert transform yields the pulse intensity, which we spatially integrated along the transverse direction to obtain the power of the reflected pulse. Figure 4(e) shows this quantity as a function of the incident pulse's CEP. The temporal compression of the field cycles transforms the incident visible 1.5-cycle pulse into an attosecond pulse train even without any spectral filtering. In figure 4(g), we plot the isolation degree, i.e. the inverse of the relative power, α_{PIC} , of the most intense satellite pulse as compared to that of the central main pulse as function of the CEP. The isolation degree reaches 10 near the CEP = $3\pi/2$, i.e. the resulting reflected pulse could be categorized as an isolated attosecond pulse (with a $1/e$ -duration of 0.3 fs). Imposing symmetry around the propagation direction, we can estimate that this quasi-isolated attosecond pulse contains a 35% fraction of the incident pulse energy.

Spectral filtering by selecting only photon energies > 10 eV lets us consider the same spectral range as in the experiment (cf figure 3). As shown in figures 4(f) and (g), this transforms the reflected pulses from the PIC simulations into well isolated attosecond pulses with an isolation degree $\alpha_{\text{PIC}}^{-1} > 10$ over half the CEP range ($[5\pi/8, 13\pi/8]$), and $\alpha_{\text{PIC}}^{-1} > 25$ over an 1/4 of the CEP range ($[3\pi/4, 5\pi/4]$), still containing $\approx 1\%$ of the incident pulse energy. The 'optimal attosecond pulse' (highest peak intensity with an isolation degree > 25) is obtained for a CEP = $5\pi/4$ and has a $1/e$ -pulse-duration of 0.18 fs.

Qualitatively, these simulations show that when considering the same spectral range as in our experiment, we expect to generate either a strong single or two weaker attosecond pulses as function of the CEP. A strong satellite pulse ($\alpha_{\text{PIC}}^{-1} \leq 5$) is generated only over 1/3 of the CEP range ($[-\pi/8, \pi/2]$).

4. Discussion

Based on the results of the PIC simulations, we will in the following discuss further the possible temporal profile of the SHHG emission generated in our single-shot experiments (cf figure 3). Qualitatively, we find agreement between the simulation and our experiments in so far as both result in a large majority of driving pulse waveforms leading to a (quasi-)isolated attosecond pulse and spectral continua, and only a narrow CEP-region where two weaker attosecond pulses and therefore strongly modulated spectra are generated (cf figures 3(d) and (the) red circles in 4(g)).

For a more quantitative comparison, we note that for a given spectral modulation depth, the symmetric Fourier-limited temporal profile is that with the weakest satellite pulse intensities. Considering such a profile with a dominant central pulse symmetrically surrounded by two satellites, assumed equal to the main pulse up to a linear phase due to their relative delays and a reduced relative intensity $\alpha_0 < 0.25$, we find a spectral modulation depth $\nu = [I(\omega)_{\text{max}} - I(\omega)_{\text{min}}] / [I(\omega)_{\text{max}} + I(\omega)_{\text{min}}] = 4\sqrt{\alpha_0} / (1 + 4\alpha_0)$, where $I(\omega)$ is the spectral intensity (cf appendix). However, the PIC simulations suggest that the case of a single satellite pulse is much more realistic. For a single satellite pulse, again equal to the main pulse except for a delay and a relative intensity $\alpha_1 < 1$, we find $\nu = 2\sqrt{\alpha_1} / (1 + \alpha_1)$ (cf appendix). The same spectral modulation depth thus corresponds to a four times more intense single satellite pulse: $\alpha_1 = 4\alpha_0$. We could therefore consider an experimentally observed spectral continuum to support a very well isolated attosecond pulse (isolation degree $\alpha_1^{-1} > 25$) if the relative satellite pulse intensity in its Fourier-limited temporal intensity profile is $\alpha_0 < 1\%$. This is the case for 9 out of the 20 single-shot acquisitions considered in figure 3, i.e. an even larger fraction that is to be expected from the PIC simulations.

The strongest spectral modulation we have observed in single-shot acquisitions corresponds to $\alpha_0 < 8\%$, and therefore $\alpha_1^{-1} \approx 3$, and therefore to weaker satellite pulses than the $\alpha_{\text{PIC}}^{-1} \approx 1$ observed in the PIC simulations near CEP = 0. This could be due to our rather small sample of 20 single-shot acquisitions, which may not contain a driving pulse within the $< \pi/2$ -wide CEP range that leads to such strong satellite pulses. There are however also experimental factors that tend to generally reduce the observed spectral modulation depth even in single-shot measurements.

(i) The undesired detection of incoherent plasma emission polluting the experimental SHHG spectra is strongly reduced by gating the MCP to a 250-ns window around each laser shot, but cannot be completely removed. This limits the achievable SHHG-to-background ratio in our experiments to ~ 20 (observable with longer driver pulses where we would expect the spectral intensities to vanish entirely between the harmonic peaks). Therefore the observable spectral modulation depths are $\nu < 0.9$, and thus $\alpha_0 < 10\%$. The error induced by a possible background signal on the inferred satellite intensities α_0 is estimated in the appendix. This can however only partly explain the unexpectedly large dominance of very low spectral modulation depths in our experimental spectra.

(ii) Spatio-spectral distortions due to aberrations in the harmonic beam imaging could contribute to washing out spectral modulations.

(iii) A non-negligible contribution of the CWE mechanism to the experimentally detected SHHG emission cannot be excluded since we consider photon energies below the CWE spectral cutoff at ≈ 30 eV. The CWE-dominated SHHG emission we obtained with the shortest gradient scale length presents strong spatio-spectral distortions, very different from the smooth profiles we are concerned with in this work, obtained with the plasma density gradient scale length adjusted to $L \approx \lambda/20$. This makes us confident that we are examining clearly ROM-dominated SHHG here.

The importance of both factors (ii) and (iii) should increase in the outer parts of the harmonic spatial beam profile, since CWE typically leads to higher XUV beam divergence [4, 5]. Indeed, the experimental angle-resolved spectrum in figure 3(b) shows a decreased spectral modulation at higher divergence angles. We minimise this influence by selecting only the central 30-mrad-wide divergence cone for the analysis in figures 3(c) and (d).

5. Conclusions

In conclusion, we generated high harmonics from plasma mirrors with controlled plasma-density gradient driven by relativistic-intensity 1.5-cycle laser pulses. We observed a variation of the spectral modulation depth of the SHHG spectra which is clearly correlated to the driving pulses' CEP variations (figure 2). In single-shot measurements, we recorded XUV spectral continua supporting high-contrast isolated attosecond pulses, with an isolation degrees between 10 and 50 for the majority of the driving pulse CEPs. 2D PIC simulations corroborate this interpretation. Our experiments thus represent a significant improvement, in terms of attosecond pulse isolation degree as well as repetition rate, over previous results obtained with 2-cycle drivers at 10-Hz [3, 28], where for the majority of driving pulse CEPs, double or triple attosecond pulse trains were obtained.

The theoretically predicted percent-level attosecond-pulse generation efficiencies, combined with the possible emission of an isolated attosecond pulse even without spectral filtering, underline the potential of relativistic plasma-mirrors as high-brightness secondary sources for future experiments exploring non-linear interactions in the VUV/XUV range. We must note, however, that we have not measured the XUV flux in our experiments. Experimental laser-to-XUV conversion efficiencies measured for plasma mirror SHHG by other groups are typically $\sim 10^{-4}$ in the spectral region beyond 30 eV [2, 3, 8, 10], which is about an order of magnitude lower than the predictions of PIC simulations.

While CEP-tagging is possible even at kHz-repetition rate [38, 39], it is of course highly desirable to stabilize the driving pulse CEP at its optimal value. We have recently achieved this stabilization with our laser system [34] and are working on harnessing this progress for future SHHG experiments.

In order to increase the spectral extent of the generated XUV continua we need to increase the on-target driving intensity. This is possible by further optimizing the spatio-temporal quality of the driver pulses [31] and motivates further development of our driving laser and post-compression system towards higher output pulse energies.

Acknowledgments

This research used resources of the National Energy Research Scientific Computing Center (NERSC), a U.S. Department of Energy Office of Science User Facility operated under Contract No. DE-AC02-05CH11231. We acknowledge financial support from the Agence Nationale pour la Recherche (ANR-11-EQPX-005-ATTOLAB, ANR-14-CE32-0011-03 APERO); the *Investissements d'Avenir* program LabEx PALM (ANR-10-LABX-0039-PALM); the European Research Council (ERC Starting Grant FEMTOELEC 306708); LASERLAB-EUROPE (H2020-EU.1.4.1.2. grant agreement ID 654148), and the Région Ile-de-France (SESAME 2012-ATTOLITE).

Appendix A. Satellite pulse intensity vs. spectral modulation depth and background noise

Consider attosecond pulse profiles with the crude simplification of the main and satellite pulse having the same complex spectral amplitudes, $A(\omega)$, up to a real-valued scaling constant and a linear phase term due to their relative delay τ . For two symmetric satellites, we thus have a spectral intensity

$$\begin{aligned} I_0(\omega) &= |A(\omega) + \sqrt{\alpha_0}A(\omega)\Re(\exp[i\tau\omega] + \exp[-i\tau\omega])|^2 \\ &= A^2(\omega)[1 + 4\alpha_0 \cos^2(\tau\omega) + 4\sqrt{\alpha_0} \cos(\tau\omega)]. \end{aligned}$$

For a single satellite, we have

$$\begin{aligned} I_1(\omega) &= |A(\omega) + \sqrt{\alpha_1}A(\omega)\Re(\exp[i\tau\omega])|^2 \\ &= A_2(\omega)[1 + \alpha_1 + 2\sqrt{\alpha_1}\cos(\tau\omega)]. \end{aligned}$$

We now only consider the spectral modulation term, i.e. the part in square brackets. For $\alpha_1 < 1$ and $\alpha_0 < 0.25$, the maxima and minima of this spectral modulation are located at $\cos(\tau\omega) = 1$ and $\cos(\tau\omega) = -1$, respectively. At these points, the modulation terms take the values $I_{0,\min} = 1 + 4\alpha_0 - 4\sqrt{\alpha_0}$ and $I_{0,\max} = 1 + 4\alpha_0 + 4\sqrt{\alpha_0}$; and $I_{1\min} = 1 + \alpha_1 - 2\sqrt{\alpha_1}$ and $I_{1\max} = 1 + \alpha_1 + 2\sqrt{\alpha_1}$, which yields the spectral modulation depths ν as given in the main text :

$$\begin{aligned} \nu_0(\alpha_0) &= \frac{I_{0,\max} - I_{0,\min}}{I_{0,\max} + I_{0,\min}} = \frac{4\sqrt{\alpha_0}}{1 + 4\alpha_0}, \\ \nu_1(\alpha_1) &= \frac{I_{1\max} - I_{1\min}}{I_{1\max} + I_{1\min}} = \frac{2\sqrt{\alpha_1}}{1 + \alpha_1}. \end{aligned}$$

For an analysis of the error progression from the spectral modulation depth ν_0 to the inferred satellite intensity α_0 , we consider $\Delta\nu_0 = \frac{d\nu_0}{d\alpha_0}|_{\alpha'_0}\Delta\alpha_0$ at the inferred value α'_0 . This yields the error

$$\Delta\alpha_0 = \frac{2\alpha'_0(1 + 4\alpha'_0)}{1 - 4\alpha'_0} \frac{\Delta\nu_0}{\nu_0}. \quad (\text{A1})$$

We attribute the relative error of the spectral modulation depth of the experimental spectra, $\Delta\nu_0/\nu_0$, mainly to an incoherent background signal. While we do subtract any spectrally constant component of the background signal such that the noise-level signal at the highest photon energies is zero, there may remain a ‘bump’ of background signal under the coherent SHHG signal. This contribution, if assumed continuous and spectrally constant in the range of the harmonic signal, would decrease the measured spectral modulation depth according to $\nu_{\text{BG}} = [(I_{\max} + \Delta I_{\text{BG}}) - (I_{\min} + \Delta I_{\text{BG}})] / [(I_{\max} + \Delta I_{\text{BG}}) + (I_{\min} + \Delta I_{\text{BG}})] = (I_{\max} - I_{\min}) / (I_{\max} + I_{\min} + 2\Delta I_{\text{BG}})$. For a background signal of $\Delta I_{\text{BG}} = \beta(I_{\max} + I_{\min})$, the measured spectral modulation would thus be underestimated by a factor $(1 + 2\beta)$. Then, the relative error $\Delta\nu_0/\nu_0 = (\nu_{\text{BG}} - \nu_0)/\nu_0 = -2\beta/(1 + 2\beta)$. For an assumed background signal level of $\beta = 0.1$, which is certainly larger than what we may have in the experiment, this yields $\Delta\nu_0/\nu_0 = -1/6$. This is the value we use in equation (A1) for the error bars in figure 3(d). Since the presence of a background signal only decreases ν_0 and therefore increases α_0 , these error bars only go in the positive direction.

ORCID iD

Stefan Haessler  <https://orcid.org/0000-0002-7003-2089>

References

- [1] Tsakiris G D, Eidmann K, Meyer-ter Vehn J and Krausz F 2006 *New J. Phys.* **8** 19
- [2] Heissler P et al 2012 *Phys. Rev. Lett.* **108** 235003
- [3] Jahn O et al 2019 *Optica* **6** 280–7
- [4] Thaury C and Quéré F 2010 *J. Phys. B: At. Mol. Opt. Phys.* **43** 213001
- [5] Dromey B et al 2009 *Nat. Phys.* **5** 146
- [6] Kahaly S, Monchocé S, Vincenti H, Dzelzainis T, Dromey B, Zepf M, Martin P and Quéré F 2013 *Phys. Rev. Lett.* **110** 175001
- [7] an der Brügge D and Pukhov A 2010 *Phys. Plasmas* **17** 033110
- [8] Rödel C et al 2012 *Phys. Rev. Lett.* **109** 125002
- [9] Heissler P, Barna A, Mikhailova J M, Ma G, Khrennikov K, Karsch S, Veisz L, Földes I B and Tsakiris G D 2015 *Appl. Phys. B* **118** 195–201
- [10] Yeung M et al 2017 *Nat. Photon.* **11** 32–5
- [11] Takahashi E J, Lan P, Mücke O D, Nabekawa Y and Midorikawa K 2013 *Nat. Commun.* **4** 2691
- [12] Nayak A et al 2018 *Physical Review A* **98** 023426
- [13] Gonoskov A 2018 *Phys. Plasmas* **25** 013108
- [14] Thévenet M, Vincenti H and Faure J 2016 *Phys. Plasmas* **23** 063119
- [15] Lichters R, Vehn M t and Pukhov A 1996 *Phys. Plasmas* **3** 3425–37
- [16] Gordienko S, Pukhov A, Shorokhov O and Baeva T 2004 *Phys. Rev. Lett.* **93** 115002
- [17] Mikhailova J M, Fedorov M V, Karpowicz N, Gibbon P, Platonenko V T, Zheltikov A M and Krausz F 2012 *Phys. Rev. Lett.* **109** 245005
- [18] Gao J et al 2019 *Phys. Plasmas* **26** 103102
- [19] Calegari F et al 2012 *J. Phys. B: At. Mol. Opt. Phys.* **45** 074002
- [20] Baeva T, Gordienko S and Pukhov A 2006 *Physical Review E* **74** 065401(R)
- [21] Rykovanov S G, Geissler M, Meyer-ter Vehn J and Tsakiris G D 2008 *New J. Phys.* **10** 025025
- [22] Yeung M et al 2015 *Phys. Rev. Lett.* **115** 193903

- [23] Chen Z Y, Li X Y, Li B Y, Chen M and Liu F 2018 *Opt. Express* **26** 4572–80
- [24] Vincenti H and Quéré F 2012 *Phys. Rev. Lett.* **108** 113904
- [25] Wheeler J A, Borot A, Monchoce S, Vincenti H, Ricci A, Malvache A, Lopez-Martens R and Quere F 2012 *Nat. Photon.* **6** 829–33
- [26] Rivas D E et al 2017 *Sci. Rep.* **7** 5224
- [27] Kessel A et al 2018 *Optica* **5** 434–42
- [28] Kormin D, Borot A, Ma G, Dallari W, Bergues B, Aladi M, Földes I B and Veisz L 2018 *Nat. Commun.* **9** 4992
- [29] Albert O, Wang H, Liu D, Chang Z and Mourou G 2000 *Opt. Lett.* **25** 1125–7
- [30] Guénot D et al 2017 *Nat. Photon.* **11** 293–6
- [31] Haessler S, Böhle F, Bocoum M, Ouillé M, Kaur J, Levy D, Daniault L, Vernier A, Faure J and Lopez-Martens R 2020 arXiv:2005.01343
- [32] Jullien A, Ricci A, Böhle F, Rousseau J P, Grabielle S, Forget N, Jacqmin H, Mercier B and Lopez-Martens R 2014 *Opt. Lett.* **39** 3774–7
- [33] Böhle F et al 2014 *Laser Phys. Lett.* **11** 095401
- [34] Ouillé M et al 2020 *Light: Sci. Appl.* **9** 1–9
- [35] Bocoum M, Böhle F, Vernier A, Jullien A, Faure J and Lopez-Martens R 2015 *Opt. Lett.* **40** 3009
- [36] Goulielmakis E et al 2008 *Science* **320** 1614–17
- [37] Friedman A, Cohen R H, Grote D P, Lund S M, Sharp W M, Vay J L, Haber I and Kisker R A 2014 *IEEE Trans. Plasma Sci.* **42** 1321–34
- [38] Rathje T et al 2012 *J. Phys. B: At. Mol. Opt. Phys.* **45** 074003
- [39] Xie X et al 2012 *Phys. Rev. Lett.* **109** 243001